Supplementary Material

1 MICROTUBULE STRUCTURE AND ENERGY

At the minus end of the MT, each protofilament p starts with an alpha-tubulin at

$$\vec{m}(p,1,1) = \begin{pmatrix} R_{\mathrm{MT}} \cos\phi(p) \\ -R_{\mathrm{MT}} \sin\phi(p) \\ 3\ell_{\mathrm{t}}(p-1)/13 \end{pmatrix} \tag{S1}$$

with the mean MT radius $R_{\mathrm{MT}} = 10.5\,\mathrm{nm}$, such that the seam is located between the 13th and the 1st protofilament.

Using the direction vectors

$$\vec{d}(p,d,t) = \vec{p}(p,d,t) - \vec{m}(p,d,t) = \ell_{\mathrm{t}} \begin{pmatrix} \cos\phi(p)\sin\theta(p,d,t) \\ -\sin\phi(p)\sin\theta(p,d,t) \\ \cos\theta(p,d,t) \end{pmatrix}, \tag{S2}$$

the plus end position $\vec{p}(p,d,t)$ of any tubulin monomer can be calculated by adding all direction vectors to the minus end vector,

$$\vec{p}(p,d,t) = \vec{m}(p,1,1) + \sum_{d'=1}^{d} \sum_{t'=1}^{2} \vec{d}(p,d',t') - \delta_{t,1}\vec{d}(p,d,2). \tag{S3}$$

The protofilament length that will be used to calculate the growth and shrinkage velocities is the maximum z-coordinate of all tubulin monomers within the protofilament:

$$\ell_{\mathrm{max}}(p) = \max_{d,t} \left(\vec{p}(p,d,t) \cdot \vec{e}_z\right). \tag{S4}$$

For straight and slightly curved protofilaments, $\ell_{\mathrm{max}}(p) = \vec{p}(p,d(p),2) \cdot \vec{e}_z$ is the position of the plus end of the protofilament. For strongly curved protofilaments exhibiting a ram's horn and curling backwards, the length can exceed the z-coordinate of the terminal beta-tubulin, $\ell_{\mathrm{max}}(p) > \vec{p}(p,d(p),2) \cdot \vec{e}_z$.

In order to define the lateral bond energies between tubulin dimers in neighboring protofilaments, we need to introduce interaction points, where the harmonic springs of the lateral bonds attach. The lateral interaction points are located at the edge of the upper base at $\vec{p}(p,d,t) + \vec{c}(p,d,t)$ and $\vec{p}(p,d,t) - \vec{c}(p,d,t)$ with the connection vector

$$\vec{c}(p,d,t) = \begin{pmatrix} -r_{\mathrm{t}} \sin\phi(p) \\ -r_{\mathrm{t}} \cos\phi(p) \\ 0 \end{pmatrix}. \tag{S5}$$

The connection vector

$$\vec{s}(p,d,t) = (\vec{p}(p+1,d,t) - \vec{c}(p+1,d,t)) - (\vec{p}(p,d,t) + \vec{c}(p,d,t)) \tag{S6}$$

points from the edge of the upper base of tubulin monomer (p, d, t) to its next neighbor $(p + 1, d, t)$ and is used to define the harmonic spring energies of the lateral bonds.

2 DETAILED DYNAMICS OF SINGLE CATASTROPHES, RESCUES AND DIPS

The MT growth trajectory shown in Fig. 10(A) in the main text has two significant events: a dip at $t_{\text{sim}} = 1.2\,\text{min}$ and a catastrophe at $t_{\text{sim}} = 6.85\,\text{min}$. To determine whether newly run simulations with configurations from the initial simulation as starting points qualitatively follow the original simulation, we chose the following criteria for this particular simulation:

- To identify whether a new simulation reproduces the dip, we checked that at the end of the simulation, the MT length is at most $400\,\text{nm}$ shorter than the original simulation. As the relevant question for the dip is whether it could actually result in a catastrophe, we are only interested in the new simulations being *shorter* than the original simulation, hence there is no upper limit on the MT length difference.
- To identify whether a new simulation reproduces the catastrophe, we took the last entry in the MT length log and checked if its time t_{sim} differs less than $10\,\text{s}$ from the original simulation end and if $\ell_{\text{MT}} < 200\,\text{nm}$, i.e., if the MT continued shrinking and depolymerized (almost) completely.

For each initial configuration, we ran 20 new simulations and calculated the fraction of simulations that fulfilled the criteria above. These fractions are the probabilities for the original growth path at different points in time and they are shown color-coded in the insets (A.D) and (A.C) in Fig. 10(A).

For the analysis of Fig. 13(A) in the main text, where the hydrolysis rate is coupled to mechanics, we used the same criteria.

Figure 10(C) in the main text contains three significant events: a dip at the very beginning, a catastrophe at $t_{\text{sim}} = 9.15\,\text{min}$, and a rescue at $t_{\text{sim}} = 9.54\,\text{min}$. For this simulation, we used the following criteria:

- For the dip, we used the same criterion as before.
- For the catastrophe, we checked that after $15\,\text{s}$ (or $10\,\text{s}$ for configurations after the catastrophe), the MT was at most $400\,\text{nm}$ longer than the original MT at the same point in time.
- For the rescue, we took the last entry in the MT length log of the new simulations and checked if $t_{\text{sim}} > 59\,\text{s}$, i.e., if the new simulation finished due to the time constraint and not due to the MT having vanished meaning that the rescue actually happened.

Again, we ran 20 new simulations for each of the three initial configurations and obtained the probabilities for the simulation to follow the original growth path, which are shown as color code in the insets (C.D), (C.C), and (C.R) in Fig. 10(C). The color coding reveals that the dip in (C.D) is actually better characterized as a catastrophe immediately followed by a rescue. In addition, Fig. 10(B) shows snapshots of the MT configuration at characteristic points in the growth path, for example, before, in the middle, and after the catastrophe and rescue events.

Figure S1 shows additional data on the catastrophe and rescue events from Fig. 10 in the main text (catastrophes from insets (A.C) and (C.C) and rescue from (C.R)). We show the mean protofilament length ℓ_{MT} together with additional information on the length fluctuations σ_ℓ of the individual protofilament lengths and the average GTP-cap length N_{cap}. When catastrophes become unavoidable, the cap length has shrunken to around $N_{\text{cap}} \sim 2$, for rescues a cap length around $N_{\text{cap}} \sim 4$ seems necessary. Length fluctuations are also increased if catastrophe or rescues are triggered.

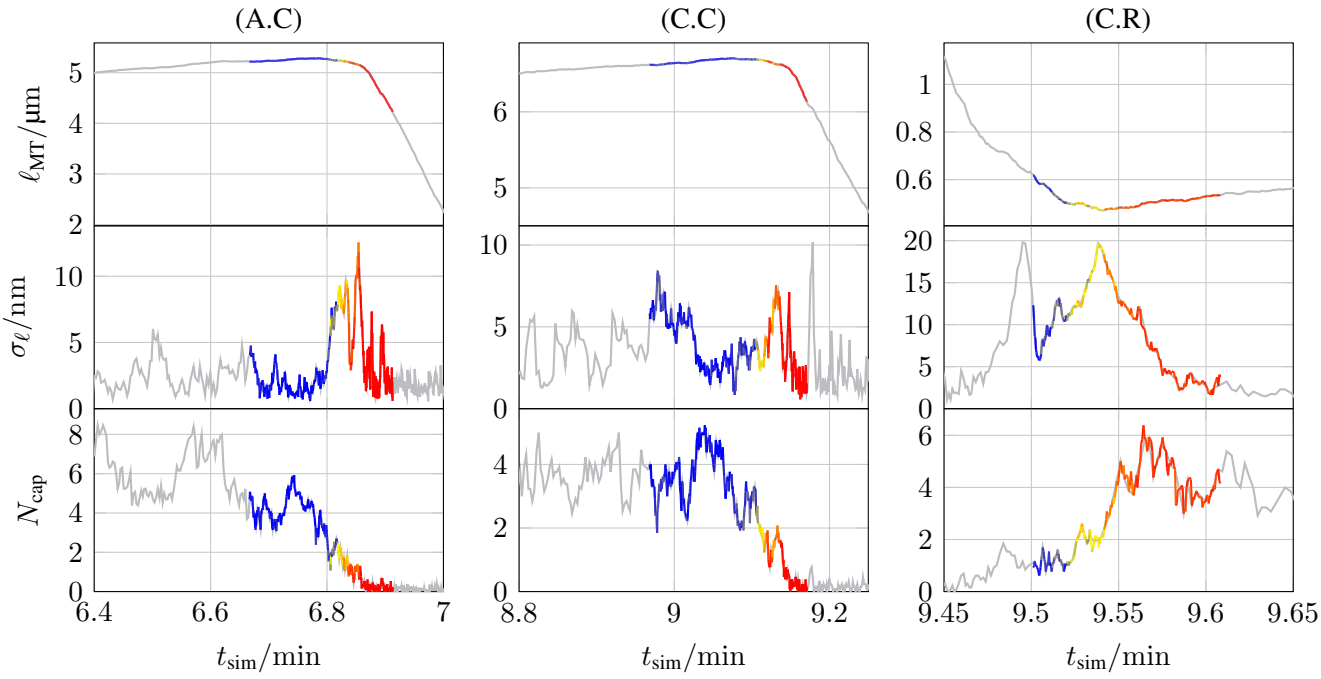

Figure S1. The standard deviation σ_ℓ of the individual protofilament lengths from the mean protofilament length ℓ_{MT} and the average cap length N_{cap} of the two catastrophes and the rescue shown in the insets of Fig. 10 in the main text as a function of simulation time t_{sim}. The same color coding as in Fig. 10 in the main text is used and gray is used to show additional data before and after the highlighted parts in the insets of Fig. 10.

3 DETERMINATION OF CATASTROPHE AND RESCUE RATES

For the determination of catastrophe and rescue rates in Fig. 8 in the main text we employed the following algorithm.

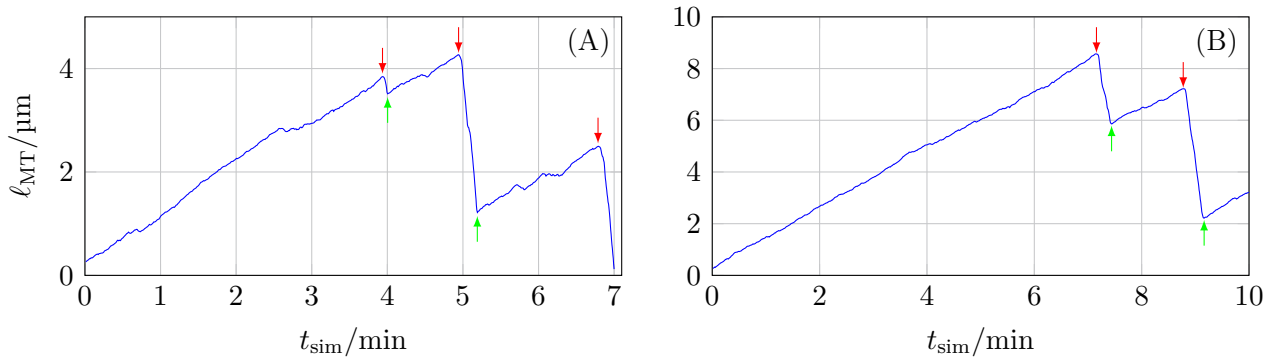

Figure S2. Two exemplary microtubule trajectories in which catastrophes and rescues determined by the algorithm are marked by red arrows pointing down and green arrows pointing up, respectively. (A) $c_{tub} = 10\,\mu M$, $k_{hydr} = 0.3\,s^{-1}$ (B) $c_{tub} = 11\,\mu M$, $k_{hydr} = 0.4\,s^{-1}$.

First a MT trajectory $\ell_{MT} = \ell_{MT}(t_{sim})$ is classified into growth and shrinkage intervals using a greedy threshold value $\Delta\ell_1 = 50\,nm$. We start at the beginning of an interval at $t_{sim} = t_0$ and increase t_{sim} searching for a suitable end t_1 of an interval. If $\ell_{MT}(t_1) - \ell_{MT}(t_0) \geq \Delta\ell_1$, i.e., if a MT has grown more

than $\Delta\ell_1$, the interval $[t_0, t_1]$ is classified as growth interval. Likewise, if $\ell_{\mathrm{MT}}(t_1) - \ell_{\mathrm{MT}}(t_0) \leq -\Delta\ell_1$, i.e., if a MT has shrunken by more than $\Delta\ell_1$, the interval $[t_0, t_1]$ is classified as growth interval. All plateaus, where the length changes by less than $\Delta\ell_1$ are "absorbed" into surrounding growth or shrinkage intervals. This part of the procedure gives a complete classification into a (not necessarily alternating) succession of growth and shrinkage intervals.

If the (n-1)-th interval is a growth (shrinkage) interval and the n-th interval a shrinkage (growth) interval the n-th interval is marked as possibly containing a catastrophe (rescue).

Then we continue with the second part of the algorithm, where we employ a less greedy threshold value $\Delta\ell_2 = 300\,\mathrm{nm}$. We search for a catastrophe time t_c and an enclosing interval $[t_{c-}, t_{c+}]$ in a potential catastrophe containing interval according to the following steps:

1. We find a $t_{c-} < t_c$ with $t_c - t_{c-} < 50\,\mathrm{s}$ and $\ell_{\mathrm{MT}}(t_c) - \ell_{\mathrm{MT}}(t_{c-}) \geq \Delta\ell_2$, i.e., the MT grows by $\Delta\ell_2$ within the previous $50\,\mathrm{s}$ or less. We select the largest t_{c-} fulfilling these criteria.
2. We find a $t_{c+} > t_c$ with with $t_{c+} - t_c < 50\,\mathrm{s}$ and $\ell_{\mathrm{MT}}(t_c) - \ell_{\mathrm{MT}}(t_{c+}) \geq \Delta\ell_2$, i.e., the MT shrinks by $\Delta\ell_2$ within the next $50\,\mathrm{s}$ or less. We select the smallest t_{c+} fulfilling these criteria.
3. Among all possible t_c in the potential catastrophe containing interval, we choose the value producing the smallest enclosing interval $[t_{c-}, t_{c+}]$ according to steps 1 and 2.

For rescues, we proceed analogously.

Two exemplary simulation trajectories that we analyzed with the algorithm are shown in Figure S2.

The algorithm identifies the points in time where catastrophes and rescues happen and, thus, also gives access to the times $\Delta t_{\mathrm{gr,k}}$ that a MT grows before the k-th catastrophe and times $\Delta t_{\mathrm{gr,k}}$ that a MT shrinks before the k-th rescue. Catastrophe and recue rates are obtained as inverse of the averaged average growth and shrinking times,

$$\omega_{\mathrm{cat}} = \left(\frac{1}{N_{\mathrm{cat}}} \sum_{k=1}^{N_{\mathrm{cat}}} \Delta t_{\mathrm{gr,k}} \right)^{-1} \tag{S7}$$

$$\omega_{\mathrm{res}} = \left(\frac{1}{N_{\mathrm{res}}} \sum_{k=1}^{N_{\mathrm{res}}} \Delta t_{\mathrm{sh,k}} \right)^{-1} . \tag{S8}$$

4 THEORETICAL SPATIAL GTP DISTRIBUTION

We employ a similar approach as Ref. Padinhateeri et al. [2012] and consider a one-dimensional MT (or single protofilament approximation) with polymerization rate k_{on}, effective depolymerization rate $\tilde{k}_{\mathrm{off}}$, and hydrolysis rate k_{hydr} (for all tubulin dimers, including the terminal one). In the steady state, the probability of the i-th tubulin dimer counted from the plus end ($i = d(p) - d + 1$) to be a GTP tubulin dimer is given by

$$p_i = q^i = \left[\frac{k_{\mathrm{on}} + \tilde{k}_{\mathrm{off}} + k_{\mathrm{hydr}}}{2\tilde{k}_{\mathrm{off}}} \left(1 - \sqrt{1 - \frac{4k_{\mathrm{on}}\tilde{k}_{\mathrm{off}}}{\left(k_{\mathrm{on}} + \tilde{k}_{\mathrm{off}} + k_{\mathrm{hydr}}\right)^2}} \right) \right]^i \tag{S9}$$

with $i = 1$ referring to the tubulin dimer directly at the plus end. As we are measuring the normalized probability $\tilde{p}_i$ with $\sum_{i=1}^{\infty} \tilde{p}_i = 1$, we have to compare our simulation results with

$$\tilde{p}_i = (1-q)q^{i-1}. \tag{S10}$$

While we have a constant polymerization rate k_{on} and hydrolysis rate k_{hydr} (with hydrolysis is not coupled to mechanics), there is no clear mapping of the effective one-dimensional depolymerization rate k_{off} to our three-dimensional modelling because lateral bond formation and rupture results in an effective depolymerization rate. When comparing our simulation results with the theoretical prediction (S10), we are using k_{off} as a fitting parameter and using k_{on} and k_{hydr} from the simulation.

Figure S3 compares the simulation results for $\tilde{p}_i$ and the theoretical prediction for different free tubulin dimer concentrations c (and thus different k_{on} values). Once c_{tub} is sufficiently large so that the MTs can reach a steady state of growth, the prediction by the one-dimensional theory matches the simulation data.

In the main text, we give

$$0 = -(k_{\text{on}} - \tilde{k}_{\text{off}})\frac{\mathrm{d}p_{\text{GTP}}}{\mathrm{d}x} - \langle k_{\text{hydr}}\rangle(x)\, p_{\text{GTP}}(x) \tag{S11}$$

for the probability $p_{\text{GTP}}(x)$ to find a GTP-dimer at distance $x = d(p) - d$ from the tip. (S11) is a continuous version (with a continuous $x \approx i - 1$) of the discrete master equation for p_i that leads to the above result (S9).

Again, a direct comparison with our data is not possible because of the unknown effective one-dimensional depolymerization rate $\tilde{k}_{\text{off}}$. However, (S11) can be rearranged for an explicit expression for $\tilde{k}_{\text{off}}$ so that we can calculate $\tilde{k}_{\text{off}}(x)$:

$$\tilde{k}_{\text{off}}(x) = k_{\text{on}} + \left(\frac{\mathrm{d}p_{\text{GTP}}}{\mathrm{d}x}\right)^{-1} \langle k_{\text{hydr}}\rangle(x)\, p_{\text{GTP}}(x). \tag{S12}$$

It should be noted that $\tilde{k}_{\text{off}}(x)$ is not the depolymerization rate of layer $x = d(p) - d$ but the depolymerization rate of the last layer calculated using the data from layer x. If our data can be described by (S11), we expect $\tilde{k}_{\text{off}}(x)$ to be independent of x.

Figure S4 shows $\tilde{k}_{\text{off}}(x)$ for both a constant hydrolysis rate and hydrolysis coupled to mechanics. The derivative was calculated using the symmetric derivative, except for the first and last values, were a forward or backward derivative was used. Ignoring numerical issues due to the discrete derivative and insufficient data statistics for larger x values, $\tilde{k}_{\text{off}}(x)$ is sufficiently independent of x showing that (S11) can also be used to describe the results of the simulations in which hydrolysis is coupled to mechanics.

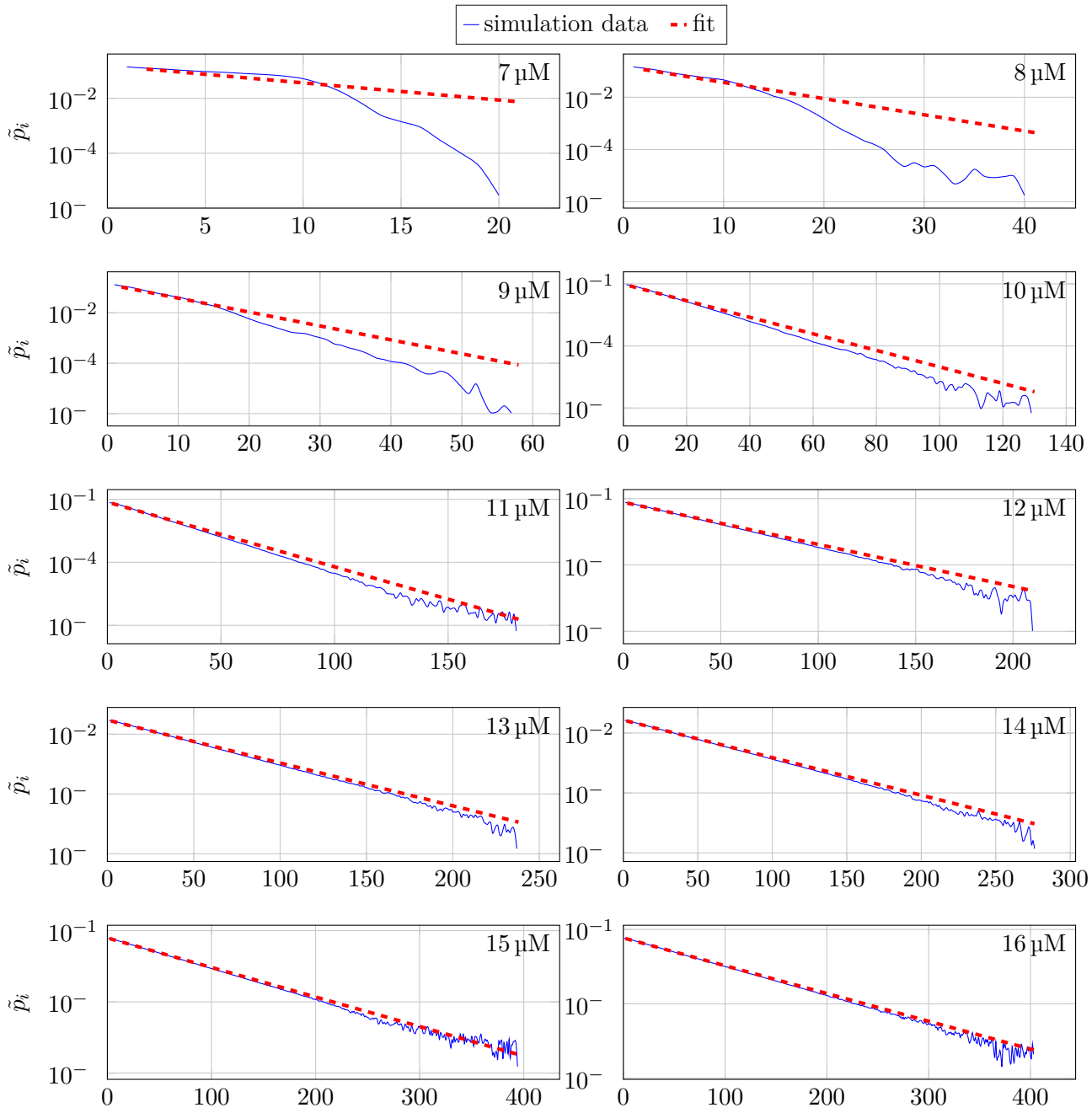

Figure S3. Relative probability $\tilde{p}_i$ of the i-th tubulin dimer counted from the plus end being a GTP-tubulin dimer with $k_+ = 4\,\mu\mathrm{M}^{-1}\,\mathrm{s}^{-1}$, $\Delta G^{0*}_{\mathrm{long}} = -9.3\,k_\mathrm{B}\,T$, $k_\mathrm{lat} = 100\,k_\mathrm{B}\,T/\mathrm{nm}^2$, and $k_\mathrm{hydr} = 0.25\,\mathrm{s}^{-1}$.

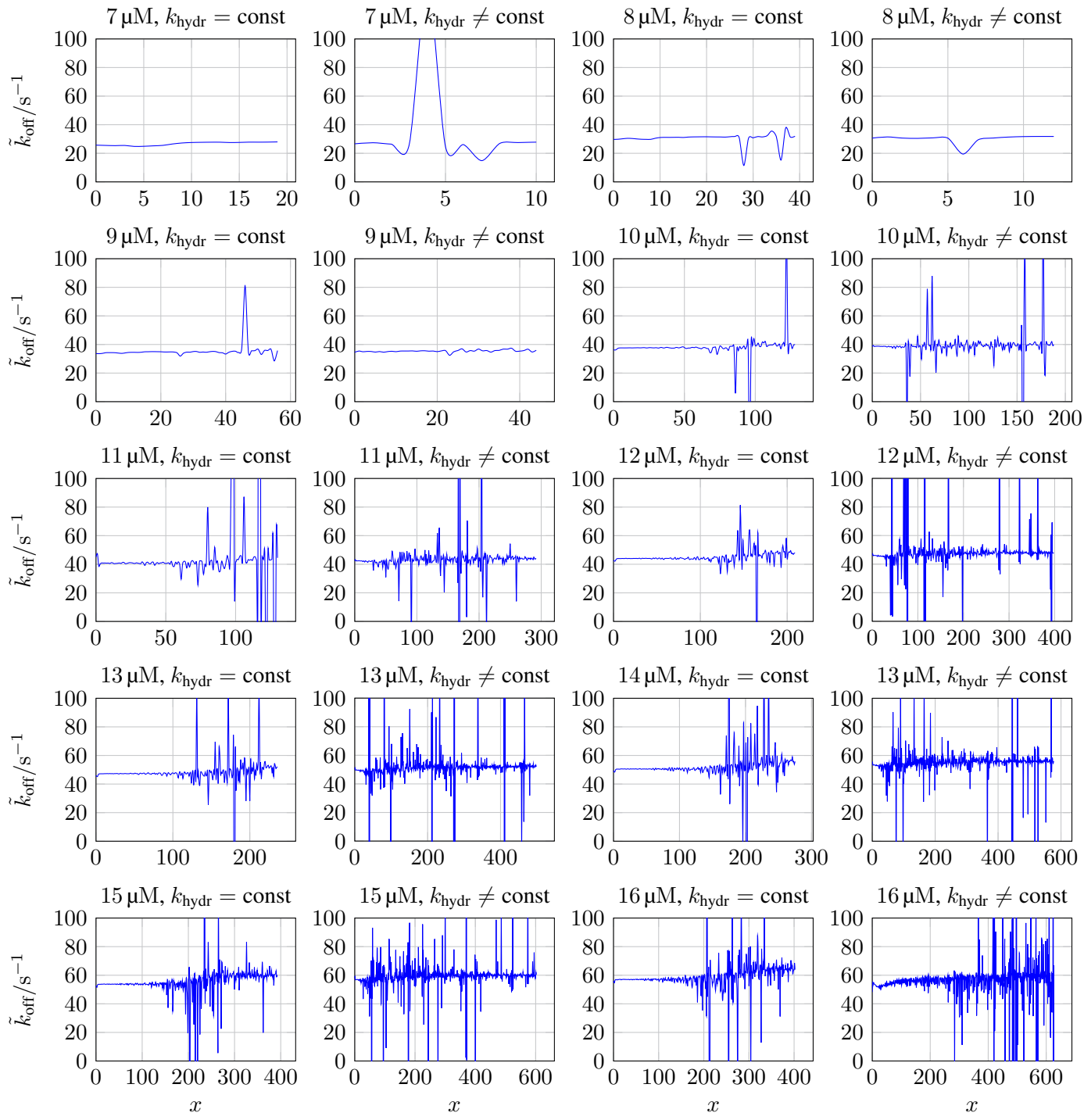

Figure S4. Depolymerization rate $\tilde{k}_{\mathrm{off}}$ calculated from the GTP-tubulin dimer probability distribution p_{GTP} according to (S12) for a constant hydrolysis rate of $k_{\mathrm{hydr}} = 0.25\,\mathrm{s}^{-1}$ and hydrolysis coupled to mechanics with $k^0_{\mathrm{hydr}} = 1.5\,\mathrm{s}^{-1}$. Values with $\tilde{k}_{\mathrm{off}} < 0\,\mathrm{s}^{-1}$ and $\tilde{k}_{\mathrm{off}} > 100\,\mathrm{s}^{-1}$ are cut off here as they are due to insufficient data statistics.

5 MINIMIZATION TIME COMPARISON BETWEEN CONSTANT HYDROLYSIS RATES AND HYDROLYSIS RATES COUPLED TO MECHANICS

To gain further insight into the additional amount of execution time required by simulations in which hydrolysis is coupled to mechanics, Figure S5 shows a comparison of average times for minimization after each of the five possible chemical events polymerization, depolymerization, bond formation, bond rupture, and hydrolysis.

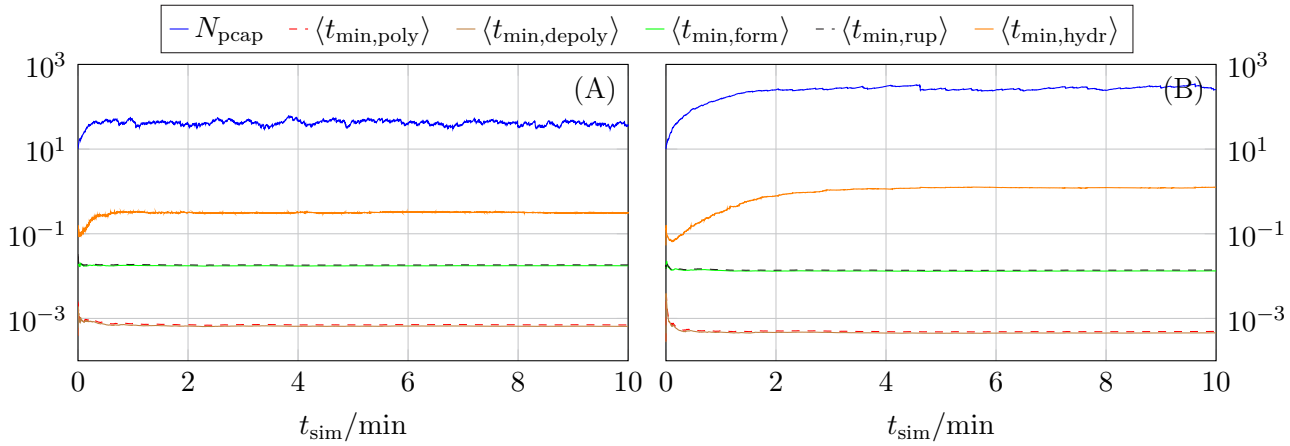

Figure S5. Comparison of the porous cap length N_{pcap} and the cumulative running averages $\langle t_{\text{min},i} \rangle$ (in seconds) for minimization times after event i for (A) a constant hydrolysis rate $k_{\text{hydr}} = 0.25\,\text{s}^{-1}$ (run on a single core of an Intel Xeon CPU E5-2650 (Sandy Bridge) processor) and (B) hydrolysis coupled to mechanics with $k^0_{\text{hydr}} = 1.5\,\text{s}^{-1}$ (run on an single core of a Intel Xeon CPU E5-2630 v3 (Haswell) processor). Both plots show the results of one exemplary simulation that use $k_+ = 4\,\mu\text{M}^{-1}\,\text{s}^{-1}$, $\Delta G^{0*}_{\text{long}} = -9.3\,k_{\text{B}}\,T$, $k_{\text{lat}} = 100\,k_{\text{B}}\,T/\text{nm}^2$, and $c_{\text{tub}} = 11\,\mu\text{M}$.

While the average minimization time after polymerization, depolymerization, bond formation, and bond rupture is not affected by mechanical feedback, the average minimization time after hydrolysis increases in the presence of mechanical feedback. In both cases, at a certain point that roughly matches the point in time when the porous cap length N_{pcap} reaches it steady state, the average minimization time after hydrolysis does not change significantly anymore either. For the two simulations shown in Figure S5, minimizations after hydrolysis take four times longer for hydrolysis coupled to mechanics than for a constant hydrolysis rate; the reason for this increase is that the porous cap length is on average more than six times longer such that minimization has to be executed for up to six times more layers if a dimer deep in GDP-body is hydrolyzed. In both cases, the simulation spends around $98\,\%$ of its time during minimization. Of that total minimization time, the simulation shown in Figure S5(A) uses roughly $30\,\%$ for minimizations after hydrolysis events, while simulation Figure S5(B) uses about $66\,\%$ for minimizations after hydrolysis events even though the difference between the percentage of hydrolysis events from all events only increased by little more than 0.1 percentage points.

6 ANALYSIS OF DILUTION SIMULATIONS

For the determination of the delay time Δt_{delay} after GTP-tubulin dilution at time t_{dil}, we employed the following algorithm.

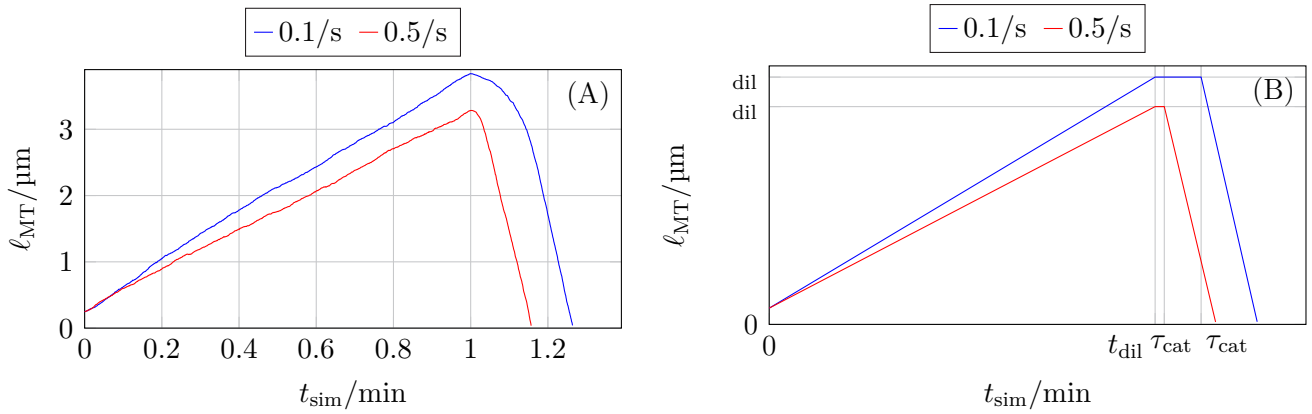

Figure S6. Example of how (A) actual microtubule growth trajectories of dilution simulations with $c_{\mathrm{tub}} = 16\,\mu\mathrm{M}$ and $c_{\mathrm{dil}} = 0\,\mu\mathrm{M}$, and two different values of k_{hydr} are simplified into (B) a growth, delay, and shrinkage phase.

First, we fit a linear growth law $\ell_{\mathrm{MT}}(t_{\mathrm{sim}}) = v_{\mathrm{gro}} t_{\mathrm{sim}} + \ell_{\mathrm{MT}}(0)$ to the MT length data for simulation times $t_{\mathrm{sim}} \leq t_{\mathrm{dil}}$ up to the dilution. This determines $\ell_{\mathrm{MT}}(t_{\mathrm{dil}})$. Then we fit a linear shrinking law $\ell_{\mathrm{MT}}(t_{\mathrm{sim}}) = v_{\mathrm{shr}}(t_{\mathrm{sim}} - \tau_{\mathrm{cat}}) + \ell_{\mathrm{MT}}(t_{\mathrm{dil}})$ ($v_{\mathrm{shr}} < 0$) to the shrinking part of the trajectory after dilution and delay. This determines the catastrophe time $\tau_{\mathrm{cat}} > t_{\mathrm{dil}}$ as intersection point with the dilation plateau $\ell_{\mathrm{MT}}(t_{\mathrm{sim}}) = \ell_{\mathrm{MT}}(t_{\mathrm{dil}})$, which we fit for $t_{\mathrm{dil}} < t_{\mathrm{sim}} < \tau_{\mathrm{cat}}$. The delay time is given by $\Delta t_{\mathrm{delay}} = \tau_{\mathrm{cat}} - t_{\mathrm{dil}}$.

Two exemplary simulation trajectories that we analyzed with the algorithm are shown in Figure S6.

7 SUPPLEMENTARY FIGURES

1. Microtubule lengths ℓ_{MT} as a function of time t_{sim} for fixed $\Delta G^{0*}_{\mathrm{long}}$, $\Delta G^{0}_{\mathrm{lat}}$, k_{att}, c_{tub}

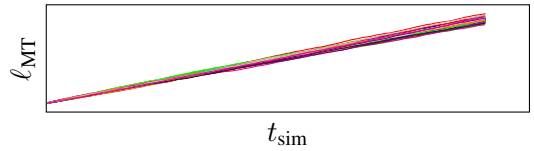

result: average growth velocity v_{gro} at c_{tub}

2. Growth velocities v_{gro} as a function of c_{tub} for fixed $\Delta G^{0*}_{\mathrm{long}}$, $\Delta G^{0}_{\mathrm{lat}}$, k_{att}

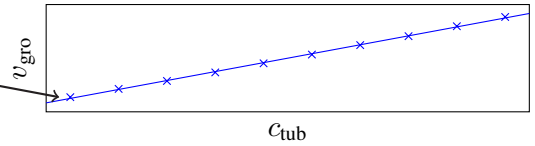

result: slope a_{gro} and intercept b_{gro} of fit $v_{\mathrm{gro}}(c_{\mathrm{tub}}) = a_{\mathrm{gro}} c_{\mathrm{tub}} + b_{\mathrm{gro}}$

3. Slopes a_{gro} and intercepts b_{gro} as a function of k_{att} for fixed $\Delta G^{0*}_{\mathrm{long}}$, $\Delta G^{0}_{\mathrm{lat}}$

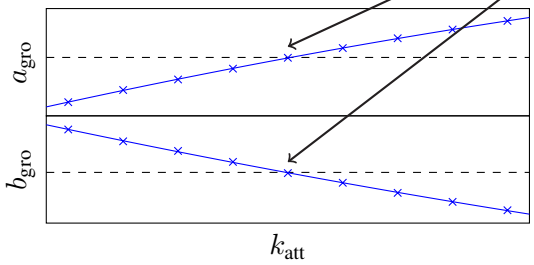

result: k_{att} that reproduces the experimental a_{gro} and b_{gro} values from Walker et al. [47] (dashed lines); only possible for one $\Delta G^{0}_{\mathrm{lat}}$ per $\Delta G^{0*}_{\mathrm{long}}$

4. $\Delta G^{0}_{\mathrm{lat}}$ and k_{lat} as a function of $\Delta G^{0*}_{\mathrm{long}}$

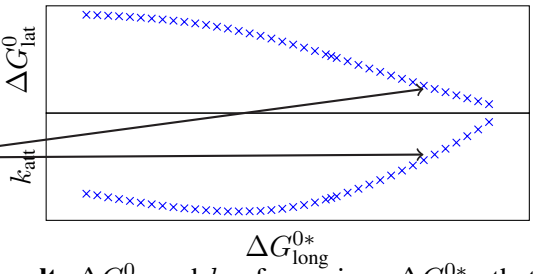

result: $\Delta G^{0}_{\mathrm{lat}}$ and k_{att} for a given $\Delta G^{0*}_{\mathrm{long}}$ that reproduce the experimental a_{gro} and b_{gro} values from Walker et al. [47]

5. Microtubule lengths ℓ_{MT} as a function of time t_{sim} for fixed $\Delta G^{0*}_{\mathrm{long}}$, $\Delta G^{0}_{\mathrm{lat}}$, k_{att}, c_{tub}, k_{lat}, κ

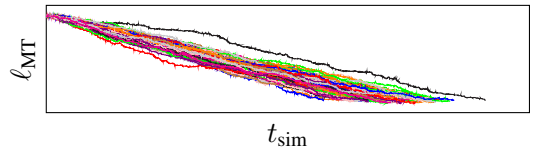

result: average shrinkage velocity v_{shr} at c_{tub}

6. Shrinkage velocities v_{shr} as a function of c_{tub} for fixed $\Delta G^{0*}_{\mathrm{long}}$, $\Delta G^{0}_{\mathrm{lat}}$, k_{att}, k_{lat} and different κ

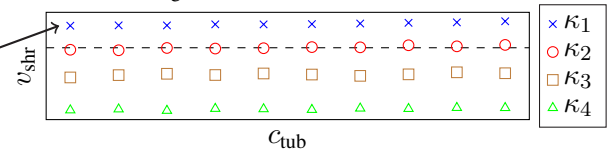

result: κ that reproduces the experimental shrinkage velocity from Walker et al. [47] (dashed line)

7. κ as a function of k_{lat} for fixed $\Delta G^{0*}_{\mathrm{long}}$, $\Delta G^{0}_{\mathrm{lat}}$, k_{att}

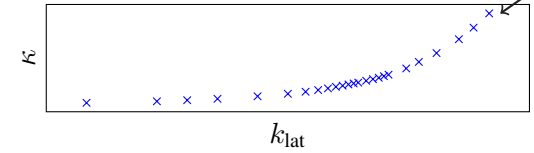

Summary

- from growth simulations: $\Delta G^{0}_{\mathrm{lat}}$ and k_{att} for a given $\Delta G^{0*}_{\mathrm{long}}$
- $\Delta G^{0*}_{\mathrm{long}}$ value that results is most linear $v_{\mathrm{gro}}(c_{\mathrm{tub}})$ in larger interval of c_{tub} values
- from shrinkage simulations: κ for a given $\Delta G^{0*}_{\mathrm{long}}$ and k_{lat}

Figure S7. Schematic illustration of how the model parameters k_{att} and $\Delta G^{0}_{\mathrm{lat}}$ as a function of $\Delta G^{0*}_{\mathrm{long}}$ (for a given k_{+}) from a large number of individual length trajectories of growing MTs (step 1) and k_{lat} as a function of κ from trajectories of shrinking MTs (step 5).

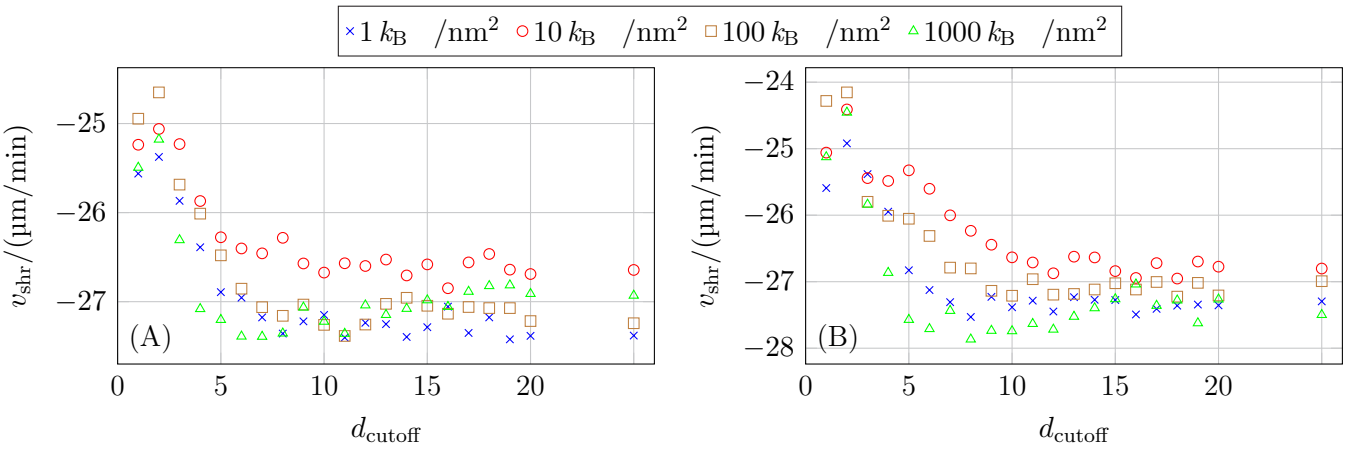

Figure S8. Influence of the minimization cutoff d_{cutoff} on the shrinkage velocity for different values of k_{lat} and (A) $k_+ = 2\,\mu\text{M}^{-1}\,\text{s}^{-1}$, $\Delta G^{0*}_{\text{long}} = -9.7\,k_B\,T$, and initial MTs consisting of $N_{\text{GDP}} = 20$ and $N_{\text{GTP}} = 0$ per protofilament, (B) $k_+ = 4\,\mu\text{M}^{-1}\,\text{s}^{-1}$, $\Delta G^{0*}_{\text{long}} = -9.3\,k_B\,T$, and initial MTs consisting of $N_{\text{GDP}} = 50$ and $N_{\text{GTP}} = 0$ per protofilament.

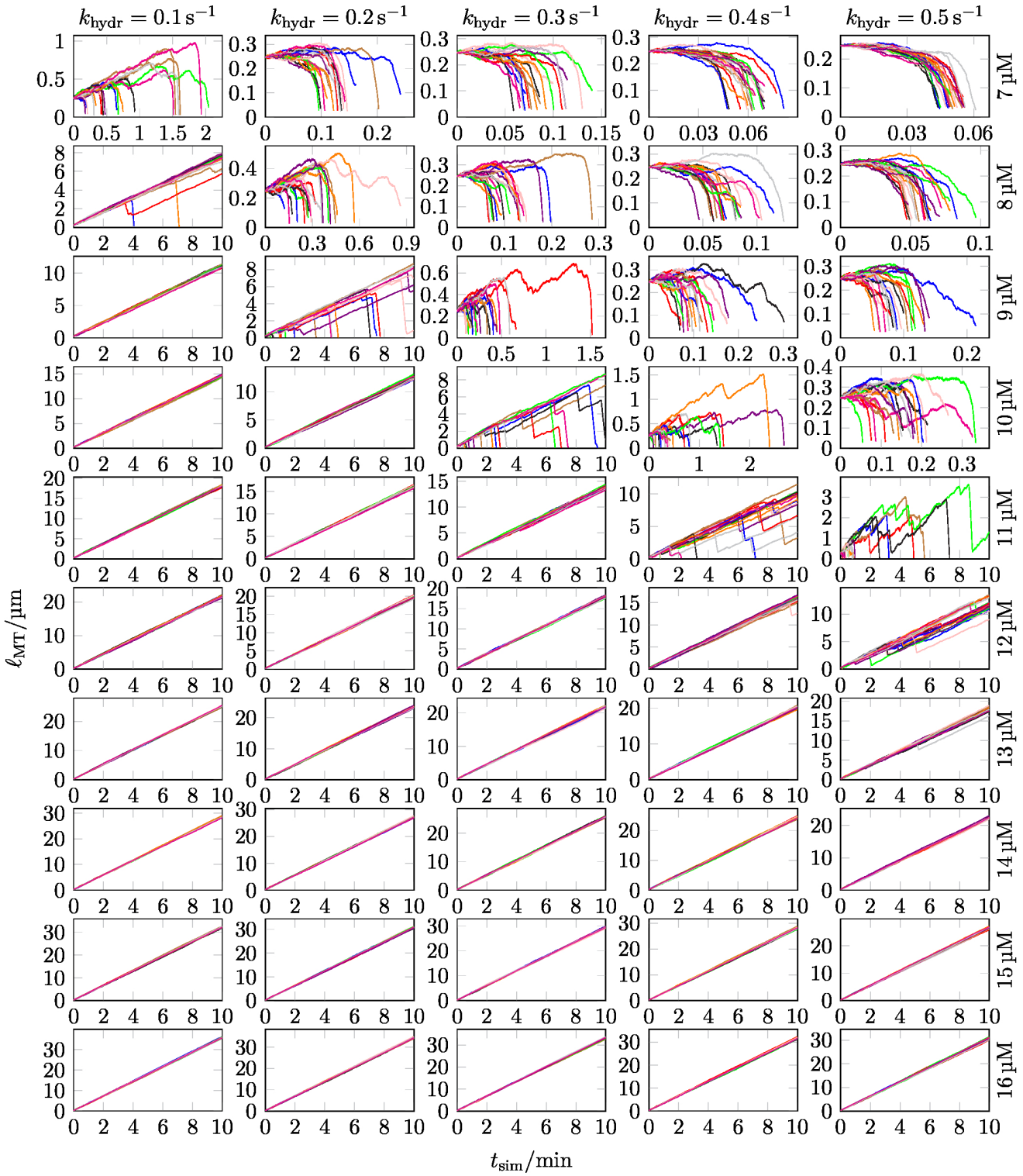

Figure S9. MT length ℓ_{MT} as a function of time t_{sim} for 20 different simulations with $k_+ = 4\,\mu\mathrm{M}^{-1}\,\mathrm{s}^{-1}$, $\Delta G^{0*}_{\mathrm{long}} = -9.3\,k_{\mathrm{B}}\,T$, $k_{\mathrm{lat}} = 100\,k_{\mathrm{B}}\,T/\mathrm{nm}^2$, ten different values of c_{tub}, and five different values of k_{hydr}. The initial MTs consist of $N_{\mathrm{GDP}} = 20$ and $N_{\mathrm{GTP}} = 10$ per protofilament. (extended version of Fig. 7 in the main text)

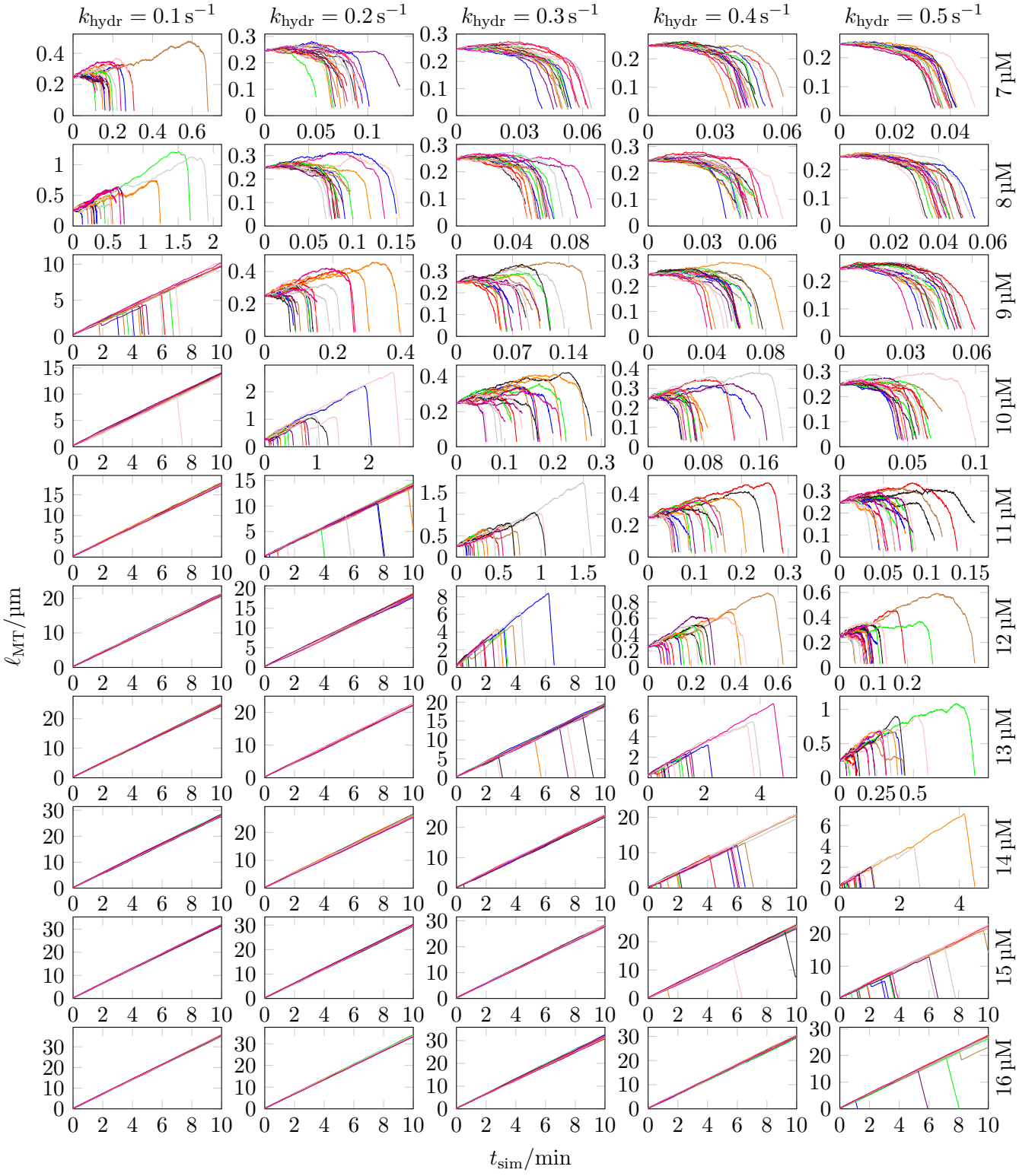

Figure S10. MT length ℓ_{MT} as a function of time t_{sim} for 20 different simulations with $k_+ = 4\,\mu\mathrm{M}^{-1}\,\mathrm{s}^{-1}$, $\Delta G^{0*}_{\mathrm{long}} = -9.3\,k_{\mathrm{B}}\,T$, $k_{\mathrm{lat}} = 1\,k_{\mathrm{B}}\,T/\mathrm{nm}^2$, ten different values of c_{tub}, and five different values of k_{hydr}. The initial MTs consist of $N_{\mathrm{GDP}} = 20$ and $N_{\mathrm{GTP}} = 10$ per protofilament.

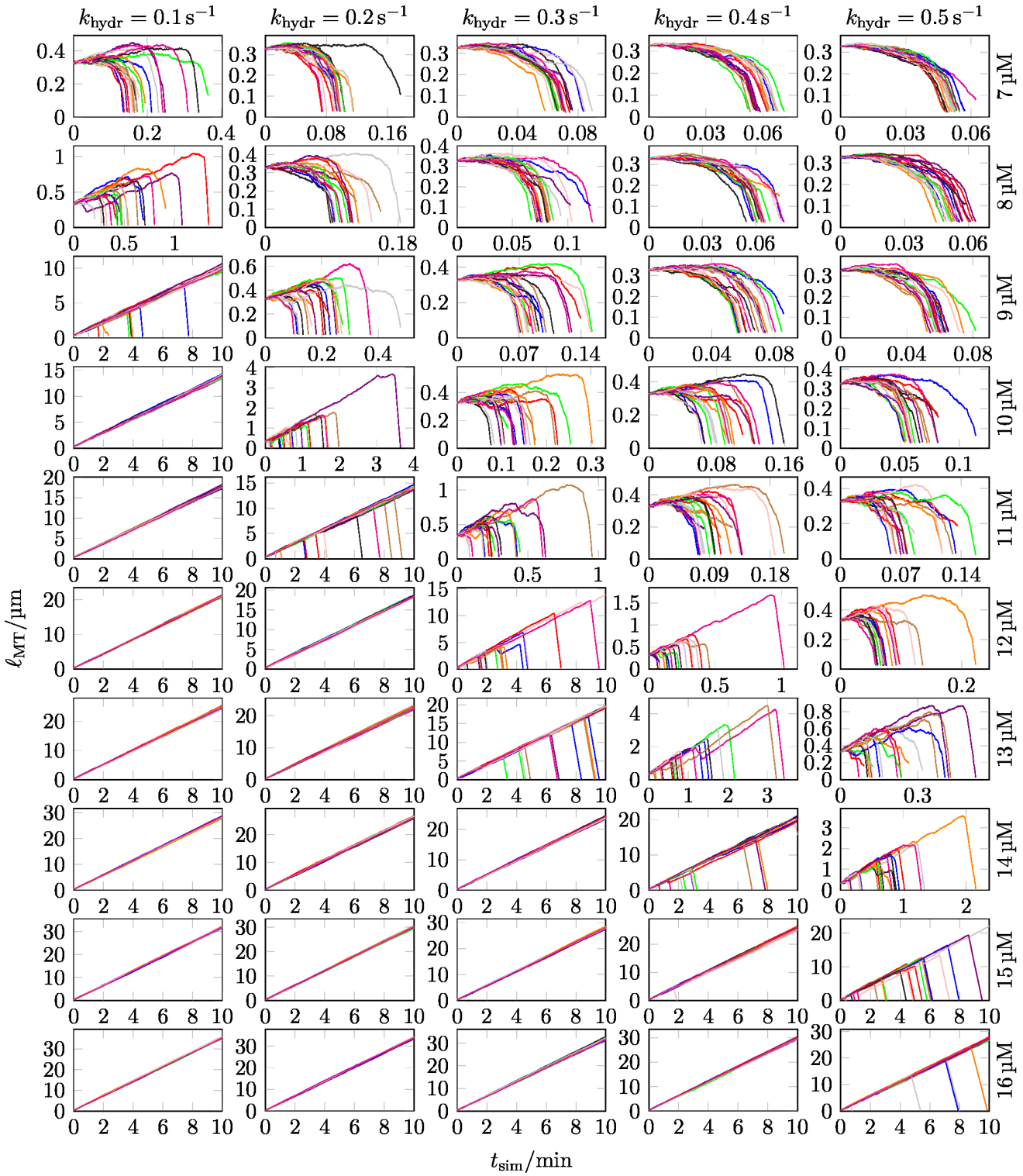

Figure S11. MT length ℓ_{MT} as a function of time t_{sim} for 20 different simulations with $k_+ = 4\,\mu\mathrm{M}^{-1}\,\mathrm{s}^{-1}$, $\Delta G^{0*}_{\mathrm{long}} = -9.3\,k_{\mathrm{B}}\,T$, $k_{\mathrm{lat}} = 1\,k_{\mathrm{B}}\,T/\mathrm{nm}^2$, ten different values of c_{tub}, and five different values of k_{hydr}. The initial MTs consist of $N_{\mathrm{GDP}} = 20$ and $N_{\mathrm{GTP}} = 20$ per protofilament.

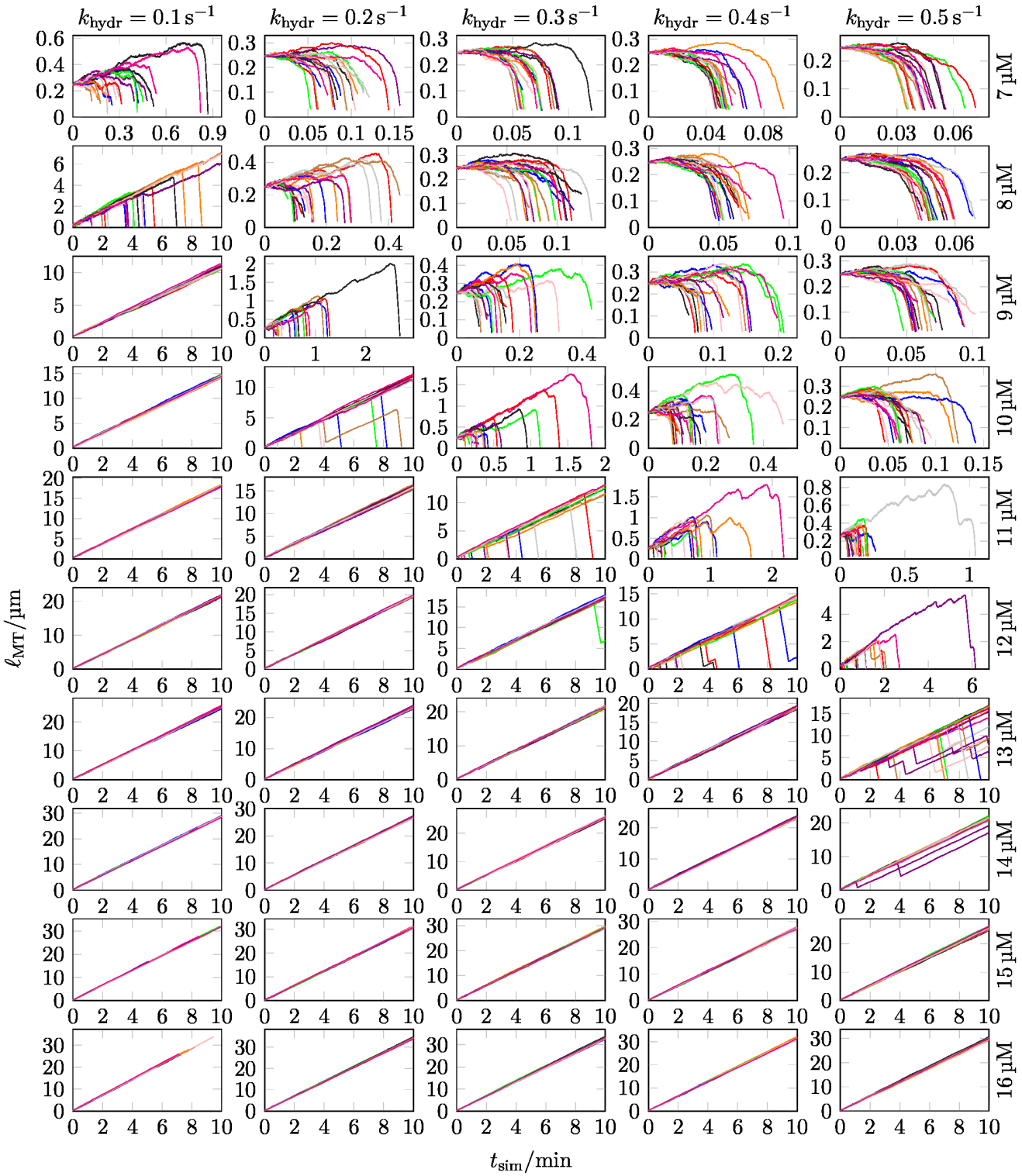

Figure S12. MT length ℓ_{MT} as a function of time t_{sim} for 20 different simulations with $k_+ = 4\,\mu\mathrm{M}^{-1}\,\mathrm{s}^{-1}$, $\Delta G^{0*}_{\mathrm{long}} = -9.3\,k_{\mathrm{B}}\,T$, $k_{\mathrm{lat}} = 10\,k_{\mathrm{B}}\,T/\mathrm{nm}^2$, ten different values of c_{tub}, and five different values of k_{hydr}. The initial MTs consist of $N_{\mathrm{GDP}} = 20$ and $N_{\mathrm{GTP}} = 10$ per protofilament. Due to runtime constraints, some of the simulations were not able to reach $t_{\mathrm{sim}} = 10\,\mathrm{min}$.

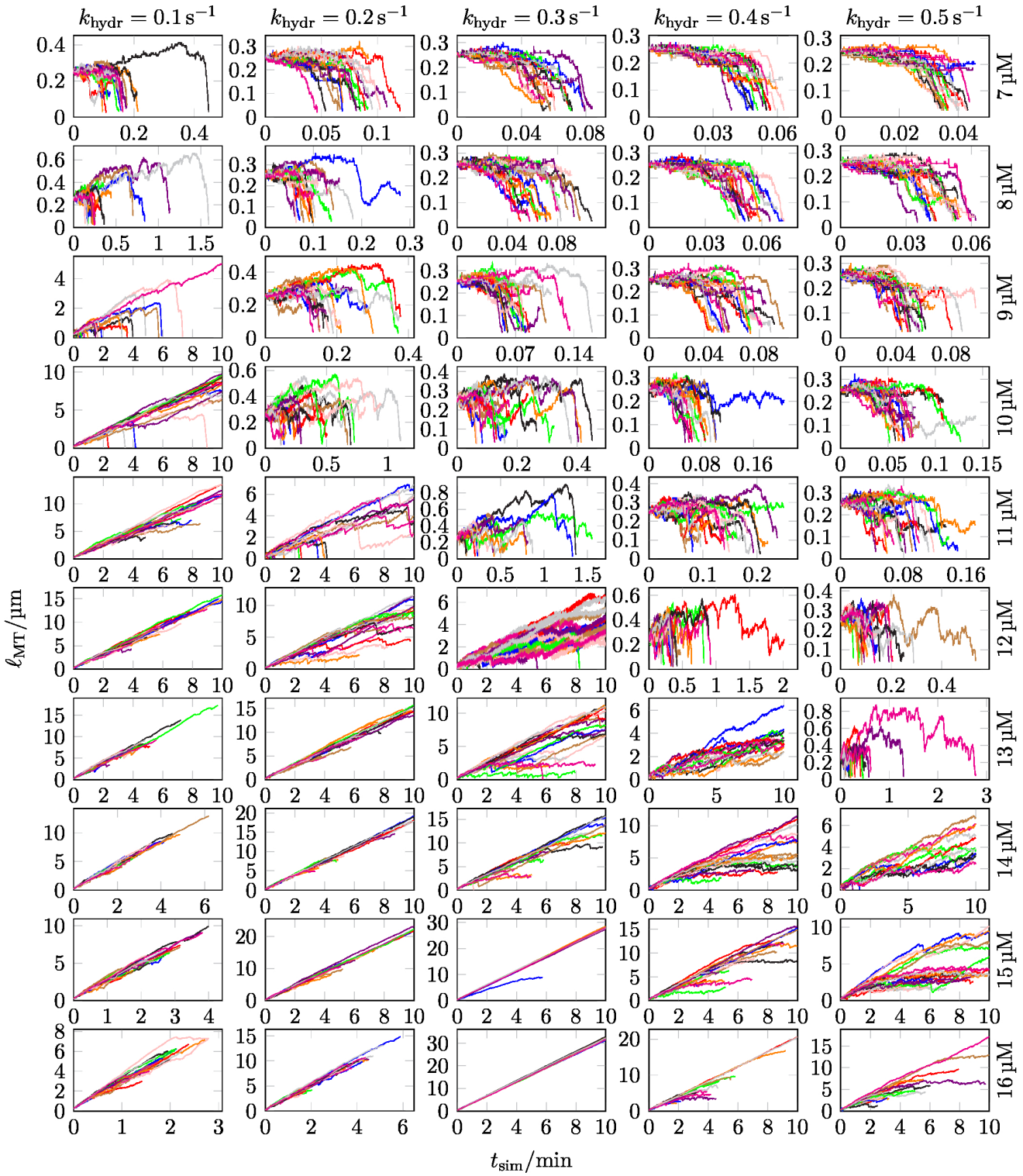

Figure S13. MT length ℓ_{MT} as a function of time t_{sim} for 20 different simulations with $k_+ = 4\,\mu\mathrm{M}^{-1}\,\mathrm{s}^{-1}$, $\Delta G^{0*}_{\mathrm{long}} = -9.3\,k_{\mathrm{B}}\,T$, $k_{\mathrm{lat}} = 20\,000\,k_{\mathrm{B}}\,T/\mathrm{nm}^2$, ten different values of c_{tub}, and five different values of k_{hydr}. The initial MTs consist of $N_{\mathrm{GDP}} = 20$ and $N_{\mathrm{GTP}} = 10$ per protofilament. Due to runtime constraints, several simulations were not able to reach $t_{\mathrm{sim}} = 10\,\mathrm{min}$.

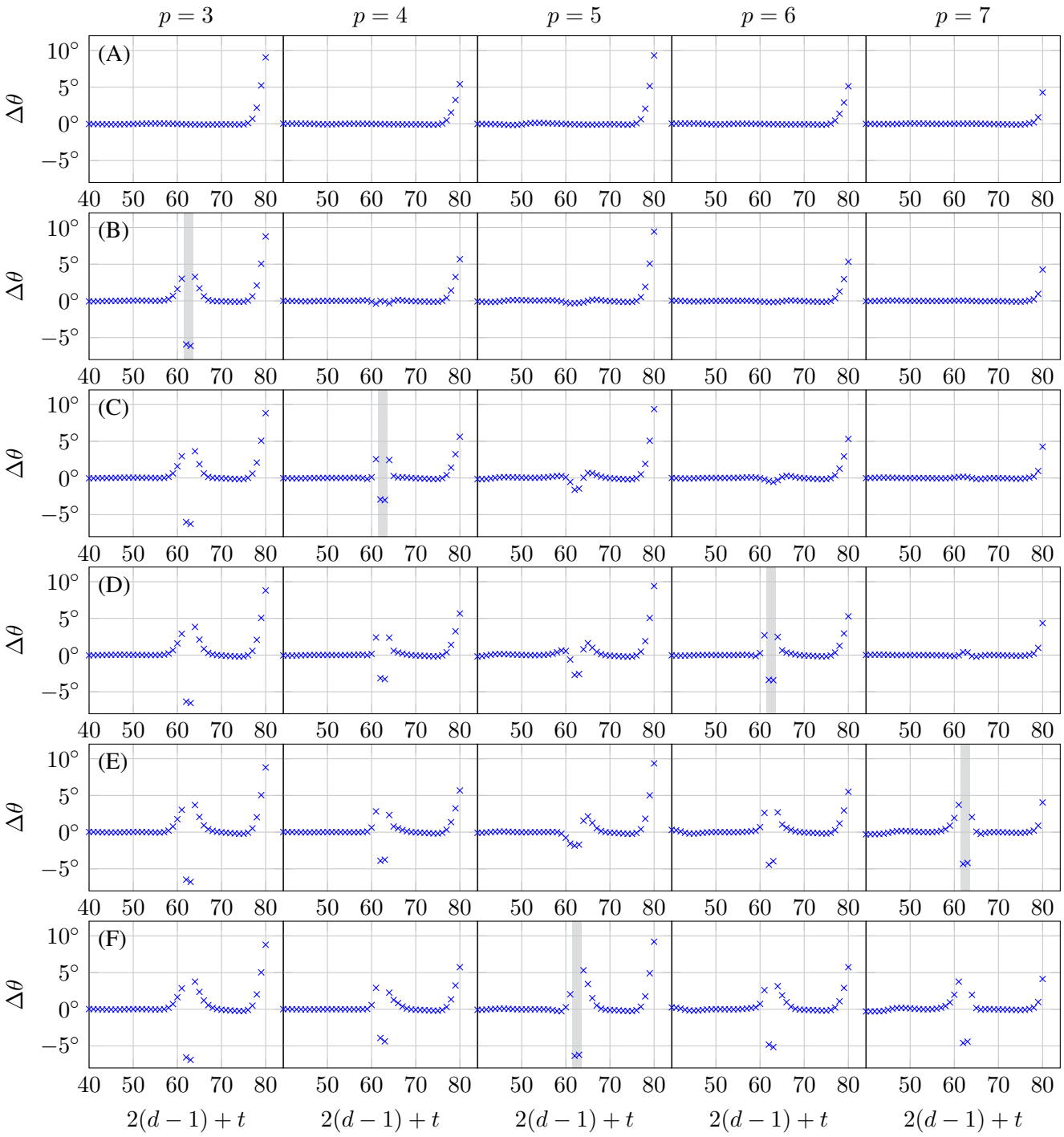

Figure S14. Influence of neighboring GTP-dimers in GDP-body on bending angles. (A) Starting from an initial MT with $N_{\text{GDP}} = 40$ and $N_{\text{GTP}} = 0$ using our standard parameter set from Table 2 in the main text, we have created a sequence in which the following GDP-dimers in layer $d = 31$ were exchanged with GTP-dimers to measure the bending angles of the GTP dimers: (B) $(3, 31)$, (C) $(4, 31)$, (D) $(6, 31)$, (E) $(7, 31)$, and (F) $(5, 31)$. The highlighted intervals show the tubulin monomers that bend inward due to all previous changes from GDP to GTP.

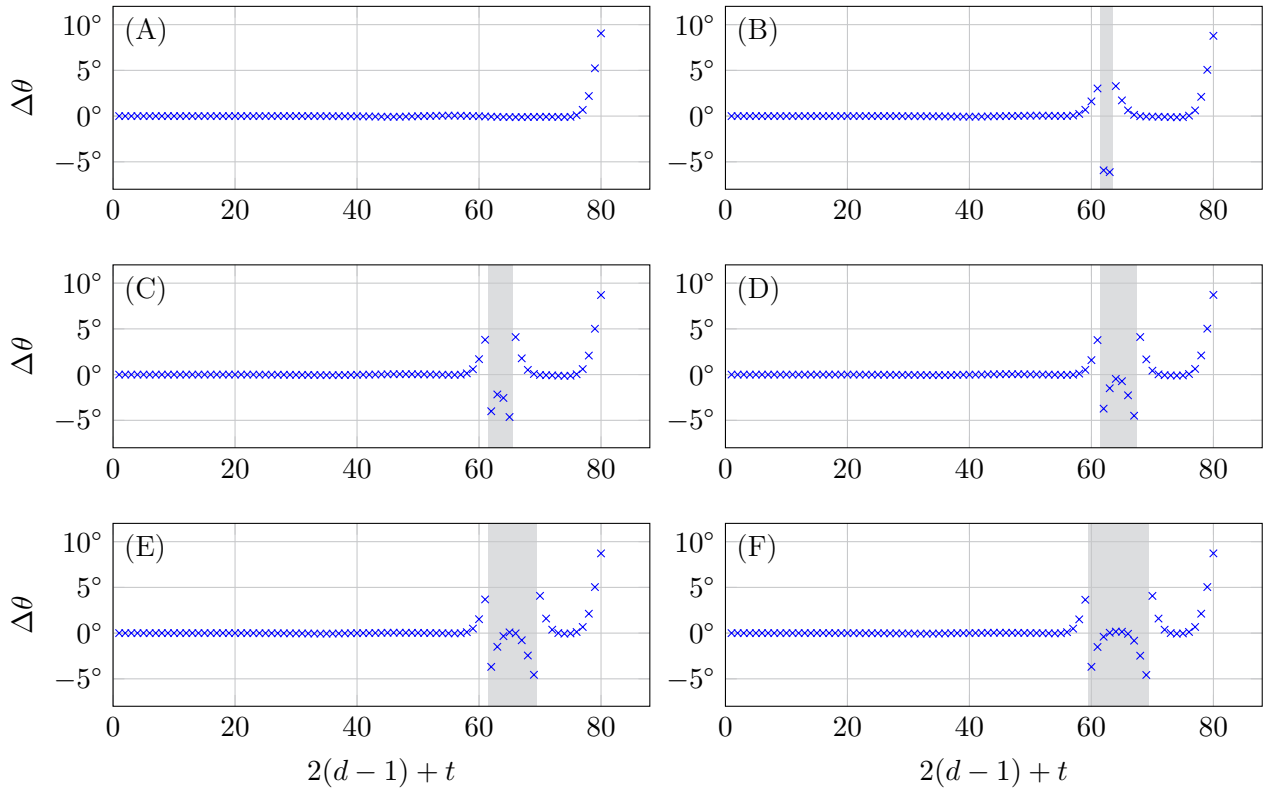

Figure S15. Influence of GTP-dimers in same protofilament in GDP-body on bending angles. (A) Starting from an initial MT with $N_{\text{GDP}} = 40$ and $N_{\text{GTP}} = 0$ using our standard parameter set from Table 2 in the main text, we have created a sequence in which the following GDP-dimers in protofilament $p = 3$ were exchanged with GTP-dimers to measure the bending angles of the GTP-dimers: (B) $(3, 31)$, (C) $(3, 32)$, (D) $(3, 33)$, (E) $(3, 34)$, and (F) $(3, 30)$. The highlighted intervals show all tubulin monomers that bend inward due to all previous changes from GDP to GTP.

8 VIDEOS

We supply videos of the microtubule (MT) growth simulations from Figs. 10 and 13 in the main text in a two- and three-dimensional representation. The videos use the following color coding:

- alpha-tubulin monomers are bright green,
- GTP-beta tubulin monomers are dark green,
- GDP-beta tubulin monomers are orange.

`MT1_2d.mp4` and `MT1_3d.mp4` show the growth of the MT from Fig. 10(A) in the main text. `MT2_2d.mp4` and `MT2_3d.mp4` show the growth of the MT from Fig. 10(C) in the main text. `MT3_2d.mp4` and `MT3_3d.mp4` show the growth of the MT from Fig. 13(A) in the main text.

REFERENCES

Padinhateeri R, Kolomeisky A, Lacoste D. Random Hydrolysis Controls the Dynamic Instability of Microtubules. *Biophys. J.* **102** (2012) 1274–1283. doi:10.1016/j.bpj.2011.12.059.

Walker RA, O'Brien ET, Pryer NK, Soboeiro MF, Voter WA, Erickson HP, et al. Dynamic instability of individual microtubules analyzed by video light microscopy: rate constants and transition frequencies. *J. Cell Biol.* **107** (1988) 1437–1448. doi:10.1083/jcb.107.4.1437.